Article

Journal of the Brazilian Chemical Society

https://dx.doi.org/10.21577/0103-5053.20240080

J. Braz. Chem. Soc. **2025**, *36*, 1, e-20240080, 1-8

Gold-Platinum Bimetallic Nanoparticles: Tailoring Plasmonic Properties through Synthesis Parameters

Franccesca Fornasier,[a] *Sthefany F. Passos,*[a] *Guilherme C. Concas,*[b] *Liying Liu,*[c] *Yutao Xing,*[d] *Tommaso Del Rosso*[b] *and Ana Maria Percebom*[*,a]

[a]*Departamento de Química, Pontifícia Universidade Católica do Rio de Janeiro (PUC-Rio), 22451-900 Rio de Janeiro-RJ, Brazil*

[b]*Departamento de Física, Pontifícia Universidade Católica do Rio de Janeiro (PUC-Rio), 22451-900 Rio de Janeiro-RJ, Brazil*

[c]*Centro Brasileiro de Pesquisas Físicas (CBPF), 22290-180 Rio de Janeiro-RJ, Brazil*

[d]*Laboratório de Microscopia Eletrônica de Alta Resolução, Centro de Caracterização Avançada para Indústria de Petróleo (LaMAR/CAIPE), Universidade Federal Fluminense (UFF), 24210-346 Niterói-RJ, Brazil*

Gold and platinum bimetallic nanoparticles, Au@PtNPs, have gained attention due to their plasmonic properties. The controlled synthesis of Au@PtNPs involves complex parameters, and the resulting synergy between Au and Pt introduces possibilities for tailoring their properties. This study explores the effects of key-parameters of synthesis (gold core diameters, reaction time, and Pt concentration) on the final properties of Au@PtNPs. Gold nanoparticles of varying diameters were synthesized and used as cores for the reduction of hexachloroplatinic acid, forming a surrounding shell of Pt nanoparticles. The parameters were systematically tuned to understand their impact on morphology, dimension, stability, and plasmonic properties of Au@PtNPs. Increasing Pt precursor concentration resulted in thicker and denser Pt shells, broadening the localized surface plasmon resonance (LSPR) band and improving Au@PtNPs stability. These properties are essential for applications such as photothermal treatment. The synthesis achieved satisfactory products within just 1 h of Pt^{4+} reduction at mild temperature without using surfactants. Only limited changes in plasmonic properties were observed after 4 h of synthesis, suggesting an optimal reaction period. Manipulating Au core diameter provided LSPR band control, with smaller cores exhibiting greater broadening towards the infrared region. This systematic exploration provided valuable insights for understanding key-parameters governing the synthesis and properties of Au@PtNPs.

Keywords: core-shell, nanotechnology, optical properties, bimetallic nanoparticles

Introduction

Gold and platinum bimetallic nanoparticles have garnered scientific interest due to the possibility of an alternative control of the localized surface plasmon resonance (LSPR) compared to single-metal nanoparticles, presenting considerable potential across various applications.[1-11] The remarkable optical properties of these nanoparticles arise from the LSPR, driven by the collective oscillation of electrons in the conduction band of metallic nanoparticles.[12,13] In the case of single-metal nanoparticles, LSPR is intricately related to the dimension, shape, and nature of metal.[14] However, the coupling of two noble metals introduces a synergistic effect on the LSPR phenomenon, altering the final properties of the nanoparticles, also depending on the relative concentration of the two metals and their morphology (e.g., core-shell, multi-shell, Janus, homogeneous alloy, decorated), resulting in different effective optical properties.[15-17] Specifically, in nanoparticles with a gold core decorated by a platinum shell (Au@PtNPs), the intensity of dipolar plasmon oscillations of Au is reduced due to the lower conductivity of Pt at optical frequencies. This reduction broadens the LSPR band, extending it towards the infrared region.[18,19]

*e-mail: apercebom@puc-rio.br
Editor handled this article: Izaura C. N. Diógenes

The synthesis of Au@PtNPs involves several parameters, including the type and concentration of the Pt precursor, the morphology of the Au core or the concentration of Au precursor, the reaction duration, and temperature.[8,10,18-21] There are two main ways to synthesize bimetallic nanoparticles: the simultaneous reduction of two metallic precursors and a two-step process involving pre-synthesized cores followed by the reduction of the second metal. The simultaneous reduction method usually forms a gold core with a dendritic platinum shell because Au^{3+} has a lower reduction potential than Pt^{4+} and reacts first.[18,19] Previous studies[18,19] indicate that the type and concentration of Pt precursor affects the LSPR band broadening. However, the simultaneous reduction method lacks control over core morphology and size.

In contrast, two-step procedures allow for precise control over the Au core before starting Pt reduction, using gold nanoparticles (AuNPs) of diverse sizes and shapes, such as spheres,[2,3] triangular nanoprisms,[22-24] multibranched nanoparticles,[8,10] nanorods[21] and nanocubes.[21] However, variations in the conditions of the reported procedures hinder a systematic comparison.

This study aims to synthesize spherical AuNPs of different dimensions to serve as cores for the reduction of $H_2PtCl_6.6H_2O$ at varying concentrations and reaction periods. The goal is to systematically investigate the impact of each parameter on the morphology, dimensions, stability, and plasmonic properties of the resulting Au@PtNPs. This exploration can serve as a means to control the specific properties of the nanoparticles, addressing a diverse range of applications.

Experimental

Materials

Hydrochloric acid (HCl, 37.0%), nitric acid (HNO_3, 65.0%), gold(III) chloride trihydrate ($HAuCl_4 \cdot 3H_2O$, 99.9%), ascorbic acid (AA, 99.0%), hexachloroplatinic acid hexahydrate ($H_2PtCl_6.6H_2O$, 37.50% Pt basis), and tribasic sodium citrate dihydrate ($Na_3C_6H_5O_7 \cdot 2H_2O$, 99%) were purchased from Sigma-Aldrich (Burlington, United States). Ultrapure water from a system with a 0.2 nm filter and resistivity above 18.2 MΩ cm was used in the experiments. Before the experiments, all the glassware was washed with aqua regia, followed by ultrapure water.

Synthesis of AuNPs (cores)

Gold nanoparticles of 25 and 32 nm were prepared by citrate reduction under stirring and heating according to the method proposed by Bastús *et al.*[25] The obtained suspensions were centrifuged to reach a gold concentration of 1.4 mmol L^{-1}.

AuNPs of 25 nm were fragmented by the process of laser fragmentation in liquid (LFL) in the free-jet configuration proposed by Ziefuss *et al.*[26] For that, the suspension of AuNPs was exposed to a Q-smart 850 laser source (Quantel, USA), operating at a frequency of 2ω (532 nm) and a repetition rate of 10 Hz. Each laser pulse had a temporal width of 5.8 ns with an energy of 30 mJ. The laser pulse was focused to a diameter of about 2 mm over the liquid free-jet with a fluence F = 1 J cm^{-2}, and directly collected in a falcon tube. Each suspension was exposed to 20 cycles, corresponding to 400 pulses mL^{-1} and resulting in nanoparticles with an average diameter of 7 nm. Each sample was named as AuNPs(ϕ), according to their average diameter ϕ.

Hence, the syntheses provided aqueous suspensions of AuNPs(7 nm), AuNPs(25 nm), and AuNPs(32 nm) to be used as cores for the next steps.

Synthesis of Au@PtNPs (reduction of H_2PtCl_6)

For the synthesis of Au@PtNPs, 1.0 mL of $Na_3C_6H_5O_7$ (24 mmol L^{-1}) was added as a stabilizer to 1.0 mL of AuNPs (1.4 mmol L^{-1}) of different diameters (7, 25 or 32 nm). Then, different volumes (0.110, 0.170, 0.330, 0.670, and 1.00 mL) of 4.2 mmol L^{-1} $H_2PtCl_6.6H_2O$ and 3.0 mL of AA (0.1 mol L^{-1}) for AuNPs(7 or 25 nm) and 0.01 for AuNPs(32 nm) and were simultaneously added dropwise to the suspension of AuNPs. The final molar ratios of Pt/Au used in the synthesis were R = 0.33, 0.5, 1.0, 2.0 or 3.0 (Table S1, Supplementary Information (SI) section). The suspension was sonicated in an ultrasound bath (EcoSonics Q5.9, 40 kHz, 200 W) for 20 min, followed by magnetic stirring for different periods (1, 4, 6, and 24 h) at 30 °C. Afterward, the resulting suspensions were placed in Eppendorf-type microtubes and centrifuged in an IKA G-L at 15000 rpm for 20 min. The supernatant was replaced by water to stop the reaction. When the sample was kept stirring for 24 h, the reaction was not stopped because we considered all the reactants to have been consumed after this period. During the synthesis, the color of the suspension changed from deep red to black. The samples were stored in Eppendorf-type microtubes for further characterization. Bimetallic nanoparticles were named: Au(ϕ nm)@Pt(R)NPs, according to the gold core diameter, ϕ, and the Pt/Au molar ratio, R.

Characterization

Dynamic light scattering (DLS)

The hydrodynamic diameter distributions of AuNPs and Au@PtNPs were determined using a Nanopartica SZ-100 from Horiba Instruments (Kyoto, Japan). A sample volume of 0.5 mL was diluted in 1.5 mL of ultra-pure water and placed in a polystyrene cuvette with four polished faces and an optical path equal to 1.00 cm. A 10 mW laser with a wavelength of 532 nm was applied. All analyses were performed at 25.0 °C in triplicate, lasting 120 s, using an angle of 90º. The obtained autocorrelation functions were fitted with the HORIBA NextGen Project SZ-100 software for Windows to obtain distributions of hydrodynamic diameter.

Zeta potential

The zeta potential measurements of AuNPs and Au@PtNPs were measured using the same equipment and samples used for DLS. However, the samples were placed in an electrode cell (carbon, 6 mm). All analyses were performed in triplicate at 25.0 °C, and the Smoluchowski model was applied to obtain the zeta potential values.

Spectroscopy

The optical density spectra of AuNPs and Au@PtNPs were measured using a UV-Vis spectrophotometer model UV-1900i from Shimadzu (Kyoto, Japan) in a wavelength range from 400 to 1000 nm at 25 °C. The samples were placed in a disposable cuvette with a 1.00 cm optical path.

Transmission electron microscopy

A Talos F200C (Thermo Fischer Scientific, Waltham, United States) and a JEOL JEM 2100F (Akishima, Japan) transmission electron microscopes (TEM) with X-ray energy-dispersive spectroscopy (EDS, with silicon drift detector) were used at the National Nanotechnology Laboratory (CNPEM, LNNano, Campinas-SP, Brazil) and at the High-Resolution Electron Microscopy Laboratory of the Fluminense Federal University (LaMAR/CAIPE, UFF, Niterói-RJ, Brazil), respectively. The suspensions of nanoparticles were drop-casted on Cu TEM grids (ultra-thin carbon support, 400 mesh, Electron Microscopy Sciences, CF-400-Cu, Hatfield, United States). Images were acquired with an acceleration voltage of 200 kV and processed in the ImageJ® software.[27]

Results and Discussion

Characterization of AuNPs (cores)

TEM images (Figure 1a) confirm that the AuNPs are *quasi*-spherical in all the obtained samples, with average diameters ϕ = 7 ± 1, 25 ± 4, or 32 ± 6 nm, determined by counting at least 200 nanoparticles (Figure S1, SI section). Each sample was named as AuNPs(ϕ), according to their

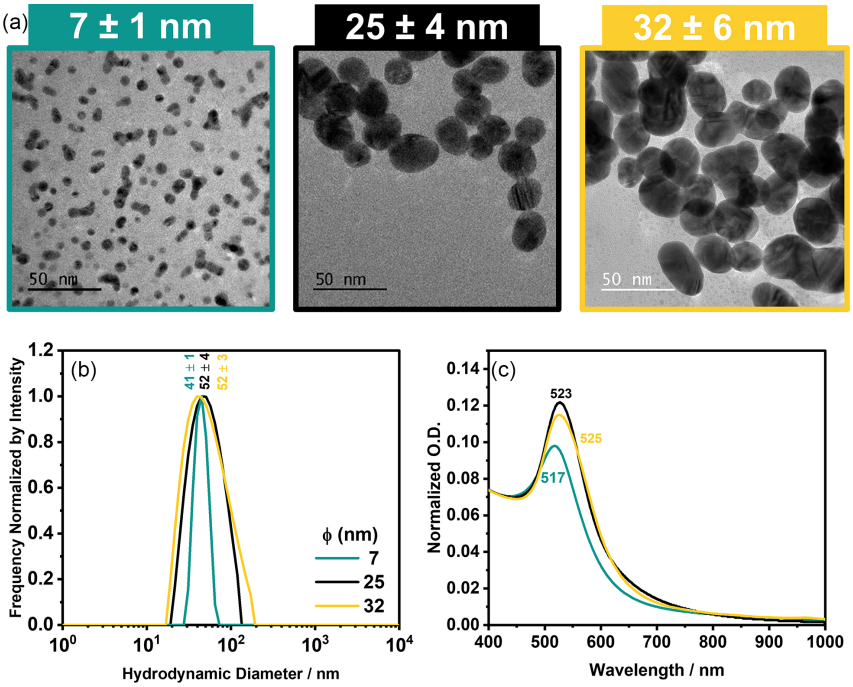

Figure 1. (a) TEM images of AuNPs with different average diameters, ϕ, (b) hydrodynamic diameter distributions (the numbers refer to the mean diameter in nm and standard deviation from triplicates), and (c) normalized optical density (O.D.) spectra of three samples (the numbers refer to the wavelength of maximum optical density). The spectra were normalized at the wavelength of 400 nm.

average diameter ϕ. DLS results confirm the formation of a monomodal distribution for all the samples of AuNPs. As expected, the hydrodynamic diameter (D_H) values are considerably higher than the diameters measured by TEM[28] (Figure 1b), and the LSPR band slightly redshifts when the average diameter increases (Figure 1c).[29] Zeta potential results (Table S2, SI section) indicate that all nanoparticles have negatively charged surfaces, favoring stability in aqueous medium.

Effect of Pt precursor concentration

The reduction of $H_2PtCl_6.6H_2O$ in the presence of AuNPs(25 nm), sodium citrate, and ascorbic acid during 24 h forms a shell of 2.5 ± 0.5 nm platinum nanoparticles (PtNPs) decorating the surface of the gold cores, resulting in Au(25 nm)@Pt(*R*)NPs (Figure 2a). Elemental mapping confirms that the cores are composed of Au (red), and the decorating shell is composed of Pt (green) (Figure 2b). Pt shells formed around Au cores are typically dendritic or consist of nanoparticles due to a lattice mismatch of 3.8% between Au and Pt.[30,31]

Increasing the concentration of $H_2PtCl_6.6H_2O$ (and *R* = Pt/Au molar ratio) makes the shell of PtNPs thicker and denser (Figure 2a). Consequently, the mean hydrodynamic diameter increases (Figure 2c), and the LSPR band broadens towards the infrared region (Figure 2d). A previous study[18] obtained Au@PtNPs using the simultaneous reduction method and also observed LSPR broadening and redshift with an increasing concentration of Pt precursor (K_2PtCl_4). However, the two-step method from the present study can form denser Pt shells than the simultaneous reduction method, which generated only branched Pt shells in the investigated concentration range.[18] Another study[20] used a two-step method to reduce H_2PtCl_6 at 100 °C in the presence of pre-synthesized AuNPs. Although it involved only two different Pt/Au molar ratios (1:1 and 2:1), results also indicated the broadening of the LSPR band with a higher concentration of Pt precursor.[20]

Red shifted LSPR bands are interesting for several applications, such as amplified optical spectroscopies,[32,33] photodynamic therapy,[34] or photothermal treatment when the plasmonic band extends up to the near-infrared region.[1,5,35] Aggregation of AuNPs can also induce broadening and redshift of the LSPR band.[36] However, the aggregates must be stable and have a controlled size for real applications, which can be challenging. Hence, obtaining Au@PtNPs with these plasmonic properties could be a relevant option. Indeed, zeta potential results (Table S2, SI section) indicate that the samples keep their surfaces negatively charged after forming the Pt shell. Au(25 nm)@Pt(0.33)NPs and Au(25 nm)@Pt(0.5)NPs precipitate after 2 months, but Au(25 nm)@Pt(1.0)NPs, Au(25 nm)@Pt(2.0)NPs and Au(25 nm)@Pt(3.0)NPs are stable for at least 12 months

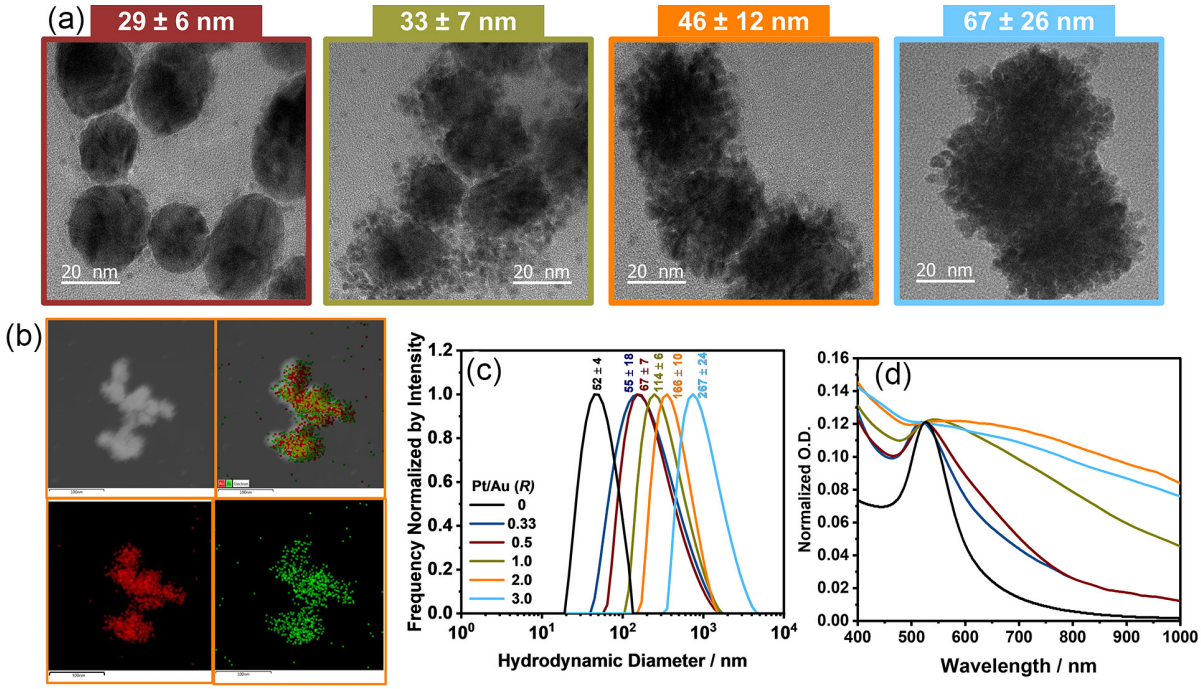

Figure 2. Results obtained for Au(25 nm)@Pt(*R*)NPs prepared with different Pt/Au molar ratios (*R*) in 24 h. (a) TEM images; (b) EDS mapping, where the first quadrant is electron image, the second quadrant is EDS layered with Au and Pt, the third quadrant is Au (red) and the fourth quadrant is Pt (green); (c) hydrodynamic diameter distributions (the numbers marked near distributions refer to the mean diameter in nm); (d) normalized optical density (O.D.) spectra. The spectra were normalized at the wavelength of 523 nm.

(Figure S2, SI section). The superior stability of systems with higher Pt/Au ratios could be related to more negative zeta potential values (electrostatic stability) or steric stability provided by the thicker Pt shells. Unlike previous studies,[1,5,37] the proposed method uses no surfactant as stabilizer, facilitating further functionalization with ligands.

Individual PtNPs are also found apart from the gold cores (Figures 2a and S3c, SI section). However, they are not observable by DLS because the hydrodynamic diameter distributions of Au(25 nm)@PtNPs exhibit only one population (Figure 2b), even when the frequency is a function of volume or number (Figure S3d). PtNPs are probably too small and diluted to present sufficient scattering intensity for detection. The individual PtNPs are formed even with low precursor molar ratios when the Pt shell is thin. Hence, an excess of Pt precursor does not induce their formation, which can be related to synthesis kinetics. We hypothesize that the initial concentration of $H_2PtCl_6.6H_2O$ probably governs the nucleation process around the gold cores, defining the thickness and density of the shells. If this hypothesis is correct, after a certain period, the continuation of the reaction should only produce more individual nanoparticles and not affect the formed Au@PtNPs anymore.

Effect of reaction time

Considering the hypothesis that Pt nucleation occurs around the gold cores and depends on the initial concentration of $H_2PtCl_6.6H_2O$, the reaction duration might be crucial in controlling the morphology and, eventually, the product properties. Typically, Au@PtNPs are obtained using high temperatures[2,18] or extended synthesis periods.[1,18,19] In this study, the syntheses of Au(32 nm)@Pt(2.0)NPs were interrupted after 1, 4, or 6 h by centrifugation and exchanging the supernatant to remove the reactants. TEM images reveal that Au(32 nm)@Pt(2.0)NPs are already formed in just 1 h (Figure 3a). Although the thickness of the shell slightly increases with time (based on the average diameters obtained by analyses of TEM images, Figure 3a), the standard deviation values indicate they are pretty similar (Figure S4, SI section). However, DLS results (Figure 3b) and O.D. spectra (Figure 3c) show a considerable change between the 1 and 4 h periods but not between 4 and 6 h. These results suggest that the present method provides Au@PtNPs in 1 h of Pt^{4+} reduction, with no substantial changes in the plasmonic properties after 4 h.

Effect of gold core diameter

One advantage of synthesizing the AuNPs before the Pt reduction is the ability to control the dimensions of the Au core. In this section, different AuNPs with diameters of ϕ = 7, 25, and 32 nm were used to prepare Au(ϕ)@Pt(2.0) NPs (Figures 4a and S5, SI section) within 4 h. DLS results confirm that the hydrodynamic diameter of Au(ϕ)@Pt(2.0) NPs increases with ϕ and that the distribution is monomodal

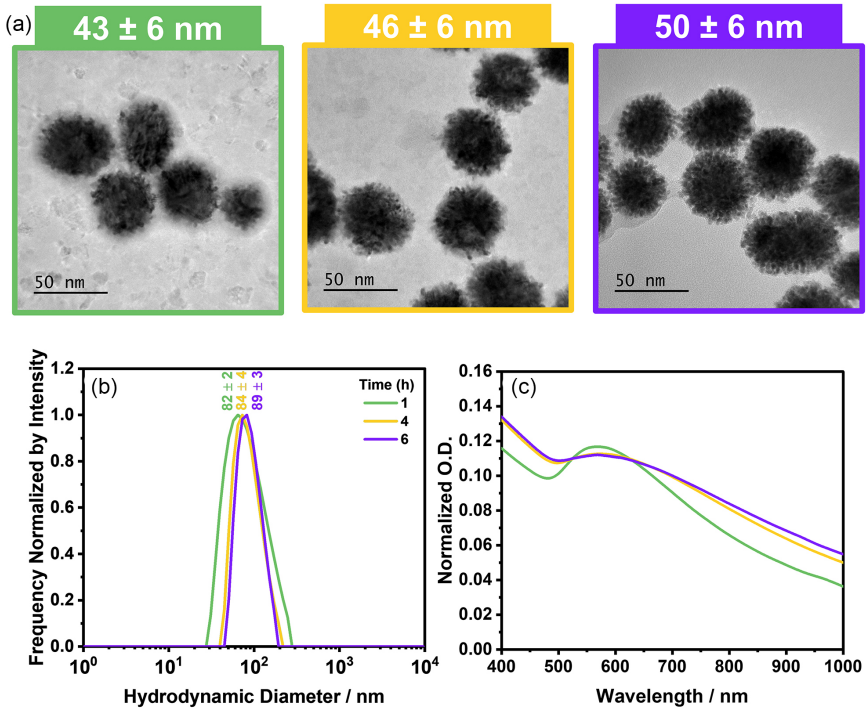

Figure 3. (a) TEM images Au(32 nm)@Pt(2.0)NPs prepared with different reaction times; (b) hydrodynamic diameter distributions (the numbers marked near distributions refer to the mean diameter in nm); (c) normalized optical density (O.D.) spectra. The spectra were normalized at the wavelength of 523 nm.

(Figure 4b). However, the hydrodynamic diameter values are considerably higher than the diameters measured by TEM, as observed for the bare AuNPs. Considering the difference in average diameters obtained by TEM for Au(ϕ)@Pt(2.0)NPs and their respective AuNPs(ϕ), the thickness of the shell increases with ϕ. Additionally, the average size of PtNPs surrounding the core is 3.3 ± 0.6, 3.6 ± 0.7, and 3.5 ± 0.7 nm for Au(ϕ)@Pt(2.0)NPs with ϕ = 7, 25, and 32 nm, respectively. Interestingly, PtNPs shells' morphology differs for nanoparticles with different core sizes (Figure 4a). Figure S6 (SI section) focuses on PtNPs with high magnification showing that they seem to merge when ϕ is 25 nm, but not for ϕ = 7 or 32 nm. The contribution of gold to the LSPR band of Au(ϕ)@Pt(2.0)NPs is more relevant for larger gold cores. Hence, smaller cores are more affected by the broadening of the LSPR band (Figure 4c). Although a previous study[20] used AuNPs of different sizes as cores to obtain Au@PtNPs, the authors did not explore the effects of size on the plasmonic properties. Therefore, to the best of our knowledge, this is the first study demonstrating how to control the broadening of the LSPR band by changing the size of AuNPs used as cores to obtain Au@PtNPs.

Conclusions

In this study, we systematically explored the synthesis and characterization of Au@PtNPs intending to tailor their optical properties, focusing on the effects of key parameters, including Pt precursor concentration, reaction time, and the diameter of the gold core. Increasing concentrations of $H_2PtCl_6.6H_2O$ led to the formation of thicker and denser PtNPs shells, resulting in the broadening of the LSPR band. The stability of the Au@PtNPs, observed over months, highlighted the potential of higher Pt/Au ratios to enhance stability, possibly attributed to more negative zeta potential values and steric stability conferred by thicker Pt shells. Our exploration into the influence of reaction time demonstrated that the synthesis of Au@PtNPs was remarkably efficient, achieving satisfactory results within just 1 h of Pt^{4+} reduction. Further analysis revealed limited changes in plasmonic properties after 4 h, suggesting an optimal reaction period for this two-step method. Moreover, by manipulating the gold core diameter, we demonstrated a novel approach to controlling the LSPR band's broadening in Au@PtNPs. Smaller cores were more susceptible to the broadening effect, a crucial insight for applications dependent on specific plasmonic properties.

This investigation provides valuable insights into the controlled synthesis of Au@PtNPs. It offers a way to tailor their characteristics to meet the demands of diverse applications, such as amplified optical spectroscopies, photodynamic therapy, or photothermal treatment. The systematic understanding of key parameters presented

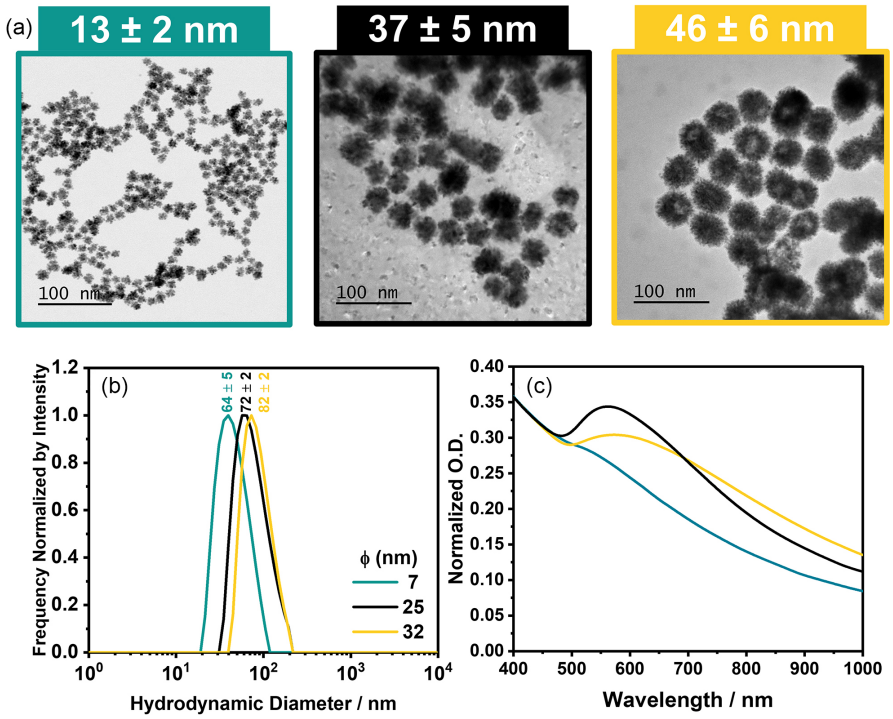

Figure 4. (a) TEM images of Au(ϕ nm)@Pt(2.0)NPs with different ϕ prepared in 4 h, where the sizes refer to the diameter considering the Pt shell; (b) hydrodynamic diameter distributions (the numbers near the distributions refer to the mean diameter in nm); (c) normalized optical density (O.D.) spectra. The spectra were normalized at the wavelength of 400 nm.

in this study lays a foundation for future research and applications in nanotechnology.

Supplementary Information

Supplementary data are available free of charge at http://jbcs.sbq.org.br as PDF file.

Acknowledgments

We thank the Laboratório Nacional de Nanotecnologia (LNNano) for the use of TEM (Proposal 20210455) and the support from the staff; Central Analítica Padre Leopoldo Hainberger from PUC-Rio for the use of the DLS instrument; and Laboratório de Química Supramolecular e Nanotecnologia (LSQN) from Universidade Federal Fluminense (UFF), especially Célia Machado Ronconi and Carolina Ligiero, for kindly providing part of the 25 nm gold nanoparticles used as core. We also acknowledge the support from the Brazilian agencies: Fundação Carlos Chagas Filho de Amparo à Pesquisa do Estado do Rio de Janeiro (FAPERJ, Auxílio ao Pesquisador Recém-contratado E-26/211.228/2019, Programa Jovem Cientista do Nosso Estado E-26/201.422/2021, Apoio a Projetos Temáticos, E-26/210.104/2020), Coordenação de Aperfeiçoamento de Pessoal de Nível Superior-Brasil (CAPES, Finance Code 001) and Conselho Nacional de Desenvolvimento Científico e Tecnológico (CNPq). FF thanks CNPq (140857/2020-6), and SFP thanks FAPERJ (E-26/205.526/2022) for their scholarships.

Author Contributions

Franccesca Fornasier was responsible for conceptualization, methodology, validation, formal analysis, investigation, data curation, writing original draft; Sthefany F. Passos for validation, investigation; Guilherme C. Concas for methodology, investigation; Liying Liu for methodology, investigation; Yutao Xing for resources, writing review and editing; Tommaso Del Rosso for resources, methodology, writing review and editing; Ana Maria Percebom for conceptualization, methodology, validation, resources, writing review and editing, supervision, project administration, funding acquisition.

References

1. Yang, Y.; Chen, M.; Wu, Y.; Wang, P.; Zhao, Y.; Zhu, W.; Song, Z.; Zhang, X.-B.; *RSC Adv.* **2019**, *9*, 28541. [Crossref]
2. Gao, Z.; Ye, H.; Tang, D.; Tao, J.; Habibi, S.; Minerick, A.; Tang, D.; Xia, X.; *Nano Lett.* **2017**, *17*, 5572. [Crossref]
3. Fu, Q.; Wu, Z.; Du, D.; Zhu, C.; Lin, Y.; Tang, Y.; *ACS Sensors* **2017**, *2*, 789. [Crossref]
4. He, W.; Han, X.; Jia, H.; Cai, J.; Zhou, Y.; Zheng, Z.; *Sci. Rep.* **2017**, *7*, 40103. [Crossref]
5. Yang, Q.; Peng, J.; Xiao, Y.; Li, W.; Tan, L.; Xu, X.; Qian, Z.; *ACS Appl. Mater. Interfaces* **2018**, *10*, 150. [Crossref]
6. Shim, K.; Lee, W. C.; Heo, Y. U.; Shahabuddin, M.; Park, M. S.; Hossain, M. S. A.; Kim, J. H.; *Sci. Rep.* **2019**, *9*, 894. [Crossref]
7. Zhu, Z.; Guan, Z.; Jia, S.; Lei, Z.; Lin, S.; Zhang, H.; Ma, Y.; Tian, Z.; Yang, C. J.; *Angew. Chem., Int. Ed.* **2014**, *53*, 12503. [Crossref]
8. Cui, Q.; Shen, G.; Yan, X.; Li, L.; Möhwald, H.; Bargheer, M.; *ACS Appl. Mater. Interfaces* **2014**, *6*, 17075. [Crossref]
9. Arockia Jency, D.; Parimaladevi, R.; Arlin Jose Amali, A.; Sathe, V. G.; Umadevi, M.; *Colloids Surf., A* **2018**, *554*, 218. [Crossref]
10. Wu, J.; Qin, K.; Yuan, D.; Tan, J.; Qin, L.; Zhang, X.; Wei, H.; *ACS Appl. Mater. Interfaces* **2018**, *10*, 12954. [Crossref]
11. Yang, L.; Chen, J.; Zhong, X.; Cui, K.; Xu, Y.; Kuang, Y.; *Colloids Surf., A* **2007**, *295*, 21. [Crossref]
12. Willets, K. A.; Van Duyne, R. P.; *Annu. Rev. Phys. Chem.* **2007**, *58*, 267. [Crossref]
13. Eustis, S.; El-Sayed, M. A.; *Chem. Soc. Rev.* **2006**, *35*, 209. [Crossref]
14. Dreaden, E. C.; Alkilany, A. M.; Huang, X.; Murphy, C. J.; El-Sayed, M. A.; *Chem. Soc. Rev.* **2012**, *41*, 2740. [Crossref]
15. Ferrando, R.; Jellinek, J.; Johnston, R. L.; *Chem. Rev.* **2008**, *108*, 845. [Crossref]
16. Srinoi, P.; Chen, Y.-T.; Vittur, V.; Marquez, M.; Lee, T.; *Appl. Sci.* **2018**, *8*, 1106. [Crossref]
17. Zhang, C.; Chen, B.-Q.; Li, Z.-Y.; Xia, Y.; Chen, Y.-G.; *J. Phys. Chem. C* **2015**, *119*, 16836. [Crossref]
18. Guo, S.; Li, J.; Dong, S.; Wang, E.; *J. Phys. Chem. C* **2010**, *114*, 15337. [Crossref]
19. Ataee-Esfahani, H.; Wang, L.; Nemoto, Y.; Yamauchi, Y.; *Chem. Mater.* **2010**, *22*, 6310. [Crossref]
20. Guo, S.; Wang, L.; Dong, S.; Wang, E.; *J. Phys. Chem. C* **2008**, *112*, 13510. [Crossref]
21. Ledendecker, M.; Paciok, P.; Osowiecki, W. T.; Pander, M.; Heggen, M.; Göhl, D.; Kamat, G. A.; Erbe, A.; Mayrhofer, K. J. J.; Alivisatos, A. P.; *Commun. Chem.* **2022**, *5*, 71. [Crossref]
22. Straney, P. J.; Marbella, L. E.; Andolina, C. M.; Nuhfer, N. T.; Millstone, J. E.; *J. Am. Chem. Soc.* **2014**, *136*, 7873. [Crossref]
23. Li, J.; Zhu, J.; Li, X.; Weng, G.; Li, J.; Zhao, J.; *Colloids Surf., A* **2022**, *653*, 130081. [Crossref]
24. Xie, X.; van Huis, M. A.; van Blaaderen, A.; *J. Phys. Chem. C* **2023**, *127*, 16052. [Crossref]
25. Bastús, N. G.; Comenge, J.; Puntes, V.; *Langmuir* **2011**, *27*, 11098. [Crossref]
26. Ziefuss, A. R.; Steenbock, T.; Benner, D.; Plech, A.; Göttlicher, J.; Teubner, M.; Grimm-Lebsanft, B.; Rehbock, C.; Comby-Zerbino, C.; Antoine, R.; Amans, D.; Chakraborty, I.; Bester,

G.; Nachev, M.; Sures, B.; Rübhausen, M.; Parak, W. J.; Barcikowski, S.; *Adv. Mater.* **2021**, *33*, 2101549. [Crossref]
27. Rasband, W. S.; *ImageJ*, 1.53k; U. S. National Institutes of Health, Bethesda, Maryland, USA, 2021.
28. Zaman, Q.; Souza, J.; Pandoli, O.; Costa, K. Q.; Dmitriev, V.; Fulvio, D.; Cremona, M.; Aucelio, R. Q.; Fontes, G.; Del Rosso, T.; *Opt. Express* **2019**, *27*, 3200. [Crossref]
29. Scaffardi, L. B.; Pellegri, N.; de Sanctis, O.; Tocho, J. O.; *Nanotechnology* **2005**, *16*, 158. [Crossref]
30. Fan, F.-R.; Liu, D.-Y.; Wu, Y.-F.; Duan, S.; Xie, Z.-X.; Jiang, Z.-Y.; Tian, Z.-Q.; *J. Am. Chem. Soc.* **2008**, *130*, 6949. [Crossref]
31. Carbone, L.; Cozzoli, P. D.; *Nano Today* **2010**, *5*, 449. [Crossref]
32. Muniz-Miranda, M.; Del Rosso, T.; Giorgetti, E.; Margheri, G.; Ghini, G.; Cicchi, S.; *Anal. Bioanal. Chem.* **2011**, *400*, 361. [Crossref]
33. Giorgetti, E.; Margheri, G.; Delrosso, T.; Sottini, S.; Muniz-Miranda, M.; Innocenti, M.; *Appl. Phys. B* **2004**, *79*, 603. [Crossref]
34. Del Rosso, T.; Louro, S. R. W.; Deepak, F. L.; Romani, E. C.; Zaman, Q.; Tahir; Pandoli, O.; Cremona, M.; Freire Jr., F. L.; De Beule, P. A. A.; De St. Pierre, T.; Aucelio, R. Q.; Mariotto, G.; Gemini-Piperni, S.; Ribeiro, A. R.; Landi, S. M.; Magalhães, A.; *Appl. Surf. Sci.* **2018**, *441*, 347. [Crossref]
35. Armanetti, P.; Chillà, A.; Margheri, F.; Biagioni, A.; Menichetti, L.; Margheri, G.; Ratto, F.; Centi, S.; Bianchini, F.; Severi, M.; Traversi, R.; Bani, D.; Lulli, M.; Del Rosso, T.; Mocali, A.; Rovida, E.; Del Rosso, M.; Fibbi, G.; Laurenzana, A.; *Adv. Sci.* **2021**, *8*, 2001175. [Crossref]
36. Costa, J.; Zaman, Q.; da Costa, K. Q.; Dmitriev, V.; Pandoli, O.; Fontes, G.; Del Rosso, T.; *Sensors* **2019**, *19*, 584. [Crossref]
37. Ataee-Esfahani, H.; Wang, L.; Yamauchi, Y.; *Chem. Commun.* **2010**, *46*, 3684. [Crossref]

Submitted: February 3, 2024
Publicado online: May 15, 2024